2019

Accounting for aboveground carbon storage in shrubland and woodland ecosystems in the Great Basin

Emily J. Fusco
University of Massachusetts Amherst

Benjamin M. Rau
USGS New England Water Science Center

Michael Falkowski
Colorado State University

Steven Filippelli
Colorado State University

Bethany A. Bradley
University of Massachusetts Amherst

esa

ECOSPHERE

Accounting for aboveground carbon storage in shrubland and woodland ecosystems in the Great Basin

EMILY J. FUSCO [1,†] BENJAMIN M. RAU,[2] MICHAEL FALKOWSKI,[3] STEVEN FILIPPELLI,[3] AND BETHANY A. BRADLEY[1,4]

[1]*Graduate Program in Organismic and Evolutionary Biology, University of Massachusetts-Amherst, Amherst, Massachusetts 01003 USA*
[2]*USGS New England Water Science Center, Northborough, Massachusetts 01532 USA*
[3]*Department of Ecosystem Science and Sustainability, Colorado State University, Fort Collins, Colorado 80523 USA*
[4]*Department of Environmental Conservation, University of Massachusetts-Amherst, Amherst, Massachusetts 01003 USA*

Citation: Fusco, E. J., B. M. Rau, M. Falkowski, S. Filippelli, and B. A. Bradley. 2019. Accounting for aboveground carbon storage in shrubland and woodland ecosystems in the Great Basin. Ecosphere 10(8):e02821. 10.1002/ecs2.2821

Abstract. Improving the accuracy of carbon accounting in terrestrial ecosystems is critical for understanding carbon fluxes associated with land cover change, with significant implications for global carbon cycling and climate change. Semi-arid ecosystems account for an estimated 45% of global terrestrial ecosystem area and are in many locations experiencing high degrees of degradation. However, aboveground carbon accounting has largely focused on tropical and forested ecosystems, while drylands have been relatively neglected. Here, we used a combination of field estimates, remotely sensed data, and existing land cover maps to create a spatially explicit estimate of aboveground carbon storage within the Great Basin, a semi-arid region of the western United States encompassing 643,500 km^2 of shrubland and woodland vegetation. We classified the region into seven distinct land cover categories: pinyon-juniper woodland, sagebrush steppe, salt desert shrub, low sagebrush, forest, non-forest, and other/excluded, each with an associated carbon estimate. Aboveground carbon estimates for pinyon-juniper woodland were continuous values based on tree canopy cover. Carbon estimates for other land cover categories were based on a mean value for the land cover type. The Great Basin ecosystems contain an estimated 295.4 Tg in aboveground carbon, which is almost double the previous estimates that only accounted for forested ecosystems in the same area. Aboveground carbon was disproportionately stored in pinyon-juniper woodland (43.7% carbon, 16.9% land area), while the shrubland systems accounted for roughly half of the total land area (49.1%) and one-third of the total carbon. Our results emphasize the importance of distinguishing and accounting for the distinctive contributions of shrubland and woodland ecosystems when creating carbon storage estimates for dryland regions.

Key words: aboveground carbon; carbon map; Great Basin; pinyon-juniper; shrubland.

Received 16 June 2019; accepted 20 June 2019. Corresponding Editor: Debra P. C. Peters.

† **E-mail:** efusco@cns.umass.edu

INTRODUCTION

Quantifying aboveground carbon stored in ecosystems is a critical component of understanding overall carbon storage and measuring carbon fluxes associated with land cover change (Houghton 2007). While dryland ecosystems make up more than 45% of land area globally (Lal 2004), aboveground carbon mapping has tended to focus on tropical and forested ecosystems (e.g., Baccini et al. 2008, Saatchi et al. 2011, Cartus et al. 2014, Hengeveld et al. 2015) because their high productivity disproportionally contributes to carbon storage. However, the amount of aboveground carbon stored on a landscape is not constant, and semi-arid ecosystems

have recently gained increased attention in global carbon cycling because of their role in driving the inter-annual variability in terrestrial carbon storage (e.g., Poulter et al. 2014, Ahlström et al. 2015, Haverd et al. 2017). In North America, semi-arid systems account for roughly 17% of the total land area (Lal 2004), but the amount of carbon stored in these woodland and shrubland ecosystems has not previously been quantified.

The Great Basin is a semi-arid region of western North America with ecosystems ranging from sparsely vegetated salt desert shrubland (*Atriplex* spp.) to sagebrush steppe (*Artemisia* spp.) and pinyon-juniper woodlands (*Pinus* spp., *Juniperus* spp.). Dominant vegetation shifts with resource availability across elevational gradients (Blaisdell and Holmgren 1984, Miller et al. 2008, Chambers et al. 2014), and ecosystems in the Great Basin are highly productive relative to other semi-arid systems (Brooks and Chambers 2011). In particular, pinyon-juniper woodlands have the potential to contribute a significant amount of aboveground carbon storage (Huang et al. 2009); however, carbon storage in woodlands is directly related to tree cover and can be highly variable in these ecosystems, even over short distances (Rau et al. 2012). To date, most carbon accounting in these woodland and shrubland systems has focused on calculating aboveground biomass and carbon at the organismal or plot scale (e.g., Rickard 1985, Rau et al. 2010). While mapping carbon storage in pinyon-juniper woodlands using remote sensing rather than field population estimates can provide the combined benefits of high spatial detail and regional-scale estimates (Chojnacky et al. 2012), most remote sensing-based studies of carbon in the Great Basin have focused on estimating expansion rates of pinyon-juniper woodlands over relatively small areas (Sankey and Germino 2008, Strand et al. 2008, Huang et al. 2009). As a result, regional estimates of aboveground carbon are lacking. Understanding current carbon storage is critical because of the numerous large-scale threats to these ecosystems, including invasive species (Bradley et al. 2006), wildfire (Balch et al. 2013), woody plant encroachment (Miller et al. 2008), and land use/land cover change (Bradley 2010). Creating a spatially explicit baseline estimate of aboveground carbon storage in this region is critical for future carbon management.

Methods used to develop large-scale carbon maps include assigning fixed carbon values based on land cover designations (termed "stratify & multiply"; Goetz et al. 2009). A stratify & multiply approach is more appropriate in cases where canopy cover estimates and/or relationships between canopy cover and aboveground carbon are unknown. In forested systems, satellite observations can more reliably estimate continuous canopy cover, which can be related to aboveground carbon storage using field measurements (termed "direct remote sensing"; Goetz et al. 2009). Direct remote sensing has been employed globally to create carbon estimates for tropical and forested regions (e.g., Baccini et al. 2008, Saatchi et al. 2011, Cartus et al. 2014).

In the United States, the National Carbon and Biomass Database leveraged ground-based data from the USDA Forest Service Forest Inventory and Analysis (FIA) and remote sensing data from the Shuttle Radar Topography Mission (SRTM) and Landsat reflectance to create a continuous estimate of aboveground biomass and carbon at 30-m resolution (Kellndorfer et al. 2013). However, this database is focused on forest carbon (Kellndorfer et al. 2013), and it is currently unknown whether the model is effective for estimating carbon in semi-arid systems like those in the Great Basin region, which often has tree cover lower than the 10–25% necessary to be considered for forest carbon monitoring.

While the majority of carbon mapping in the United States focuses on forested systems, one study (Huang et al. 2009) quantified carbon storage in pinyon-juniper woodlands on the Colorado Plateau. Huang et al. (2009) leveraged field-based measurements and remote sensing images (hyperspectral AVIRIS and multispectral Landsat), to calculate pinyon-juniper canopy cover and aboveground carbon (Huang et al. 2009). While this remains the most extensive, spatially explicit estimate of aboveground carbon to date in pinyon-juniper woodlands, it encompasses only a quarter of the Colorado Plateau and none of the Great Basin. Aerial photography (Strand et al. 2008) and Landsat imagery (Campbell et al. 2012) have also been used to map carbon in western juniper woodlands in the Pacific Northwest across limited spatial extents. There is potential to apply these remote sensing approaches for mapping carbon in the pinyon-

juniper woodlands which cover more than 15% of the Great Basin.

A comprehensive understanding of carbon stocks globally must include dryland regions like the Great Basin, which will require different methods than those used for temperate and tropical forests. Here, we leverage field-based carbon measurements, remotely sensed canopy cover estimates, and an existing land cover database to create the first spatially explicit estimates of aboveground carbon stored in the Great Basin.

Methods

Study region

Our study area encompasses the Great Basin region of the western United States. The spatial extents of this region were defined using a combination of the EPA ecoregions (U.S. Environmental Protection Agency 2013) and LANDFIRE Existing Vegetation Type (LANDFIRE.US_140EVT; Rollins 2009, LANDFIRE 2014). First, we selected EPA Level III ecoregions that are present within the Great Basin: Blue Mountains, Central Basin and Range, Columbia Plateau, Eastern Cascades Slopes and Foothills, Northern Basin and Range, and Snake River Plain. Within these Level III ecoregions, we removed Level IV subregions that had a primary designation in LANDFIRE EVT of forest, thereby focusing our analysis on subregions containing woodland and shrubland. The resulting study region spans six western U.S. states and encompasses 643,500 km^2 of semi-arid ecosystems.

Land cover classification

Aboveground carbon is expected to vary considerably with land cover class across the Great Basin. In order to assess carbon, we created a spatially explicit 30-m land cover dataset for the study region. We classified the Great Basin into seven land cover categories: pinyon-juniper woodland, three shrubland categories (low sagebrush, salt desert shrub, and sagebrush steppe), forest/woodland, non-forest, and other/excluded based on their dominant plant functional groups and their possible aboveground carbon contributions. For example, pinyon-juniper is distinct relative to the other vegetation categories because it is the only woodland system. Woodland systems may contain large amounts of aboveground carbon, but their contribution to carbon storage is dependent on tree cover which can be highly variable over short distances. The three shrubland categories were based on the dominant species assemblages which are often determined by soil factors such as salinity, pH, and depth. These three shrub communities can have considerable variation in biomass and carbon storage depending on the localized growing conditions. For example, salt desert shrub communities are typically found on alluvial features adjacent to and in low-lying areas with poor drainage where soils are saline such as playas and salt flats. The communities are typically dominated by *Atriplex* spp. or *Sarcobatus* spp., and the vegetation density and biomass can vary considerably (Tueller 1989). Low sagebrush communities are typically found on shallow, rocky, and alkaline soils that are typically too dry to support big sagebrush (McArthur and Taylor 2004). Low sagebrush communities tend to be lower in stature than big sagebrush but can vary significantly in density and biomass as well.

Land cover classifications were based on Falkowski et al. (2017*a*), who identified pinyon-juniper using object-based identification of tree crowns from aerial photographs, and the LANDFIRE Existing Vegetation Type 140 (LANDFIRE.US_140EVT; Rollins 2009, LANDFIRE 2014). LANDFIRE EVT is a U.S. national-scale land cover product that includes current vegetation information at 30-m resolution and is created using a decision tree approach based on satellite-derived predictors (Rollins 2009).

Pixels were classified as pinyon-juniper if they had >0% cover as designated by Falkowski et al. (2017*a*) or were designated as pinyon-juniper woodlands or juniper woodland and savannah in the LANDFIRE EVT group (GP_N, Rollins 2009, LANDFIRE 2014; Fig. 1). Remaining pixels were classified using LANDFIRE EVT groups (GP_N). EVT group designation is based on the National Vegetation Classification system which considers dominant and co-dominant plant species, the plant species growth forms, and regional ecology and biogeography to make a general land cover classification (Federal Geographic Data Committee 2008). We combined shrubland EVT groups into salt desert shrub, low sagebrush, and sagebrush steppe. These shrub classifications represent a potential gradient of

aboveground biomass and carbon. While the shrubland categories intuitively include vegetation groups named for the shrubs present in them, the sagebrush steppe classification also included pixels with a grassland designation. Here, grassland typically included some shrub vegetation (GAP/USGS 2016) and comprised only 1.9% of the study area. We excluded many remaining pixels with categories of low carbon consequence (primarily agriculture, introduced grass, barren, developed, and water). The few remaining pixels were classified using the LANDFIRE EVT life form (LF) and group name designations such that pixels designated as tree or had a group name (GP_N) of chaparral were placed into the forest/woodland category, while the remaining pixels designated as shrub or herb were classified as non-forest (Fig. 2). Chaparral was grouped with the woodland category because of the *Ceanothus* spp. tendency to store large amounts of carbon (Gray 1982) and grow to a treelike form (GAP/USGS 2016). For all land cover classifications except pinyon-juniper, we used a fixed estimate of carbon associated with that land cover type (stratify & multiply, sensu Goetz et al. 2009; described below in *Carbon estimation for other land covers*).

Pinyon-juniper percent cover product and validation

Because the Great Basin has little forested area, pinyon-juniper woodlands likely account for the largest portion of aboveground carbon. However, canopy cover of pinyon-juniper varies considerably across the region. Thus, a robust estimate of carbon storage in pinyon-juniper woodland should depend on canopy cover (Rau et al. 2012). Falkowski et al. (2017*a*) mapped tree canopy cover across the greater sage grouse (*Centrocercus urophasianus*) range, which covers much of the Great Basin. This map of tree canopy cover was based on identification of individual crowns by applying spatial wavelet analysis to aerial imagery acquired by the National Agriculture Imagery Program (NAIP) between 2011 and 2013. We aggregated the 1 m presence/absence maps of tree crowns into percent cover estimates at a 30-m resolution, retaining the native Universal Transverse Mercator (UTM) projection of the tiled canopy cover maps.

To validate the 30-m resolution data, we used a linear regression to compare pinyon-juniper canopy cover estimates from 265 Sagebrush Steppe Treatment Evaluation Project (SageSTEP) plots (McIver et al. 2014) to the NAIP-based models of canopy cover (Falkowski et al. 2017*a*). The 265 SageSTEP plots within the modeled canopy cover area were distributed across 14 sites in five states (Appendix S1: Fig. S1) and were surveyed in 2006–2008 within a 30 × 33 m square. Field plot corners were georeferenced using a Trimble Juno GPS unit with spatial accuracy >4 m (Trimble, Sunnyvale, California, USA). Crown cover for individual trees in each plot was measured as the longest crown diameter and the diameter perpendicular to the longest crown. Canopy cover at each plot was then calculated based on an ellipsoid with these two dimensions fit to each tree. We retained only the untreated SageSTEP control plots for our comparison to modeled canopy cover; thus, cover should not have changed substantively between the time of the survey and the aerial image collection. Although the precise center of the plots does not necessarily align with the mapped pixel, previous comparisons of FIA plots to forest cover data suggest that these small offsets do not affect the overall comparison (Zald et al. 2014).

For areas outside the extent of the pinyon-juniper product generated by Falkowski et al. (2017*a*; 56% of the study area), but designated as pinyon-juniper by LANDFIRE, we developed a canopy cover estimate based on Falkowski et al. (2017*b*; Appendix S1: Fig. S2). Falkowski et al. (2017*b*) used a stratified random sample of pixels from the Falkowski et al. (2017*a*) canopy cover map and predicted tree crown presence/absence which was then visually assessed against NAIP imagery for these samples. Samples with an accurate representation of the tree canopy were then used to train a random forest model of canopy cover based on contemporaneous Landsat imagery and topographic indices. Landsat 5, 7, and 8 images from the Tier 1 spectral reflectance product were masked for clouds, cloud shadow, and snow using the provided quality assurance band (U.S. Geological Survey 2019*a*, *b*). Seasonal medians of spectral reflectance for the original bands and three vegetation indices were included as predictors in the random forest model. The vegetation indices included the Normalized Difference Vegetation Index (NDVI; Rouse et al. 1974), Normalized Difference

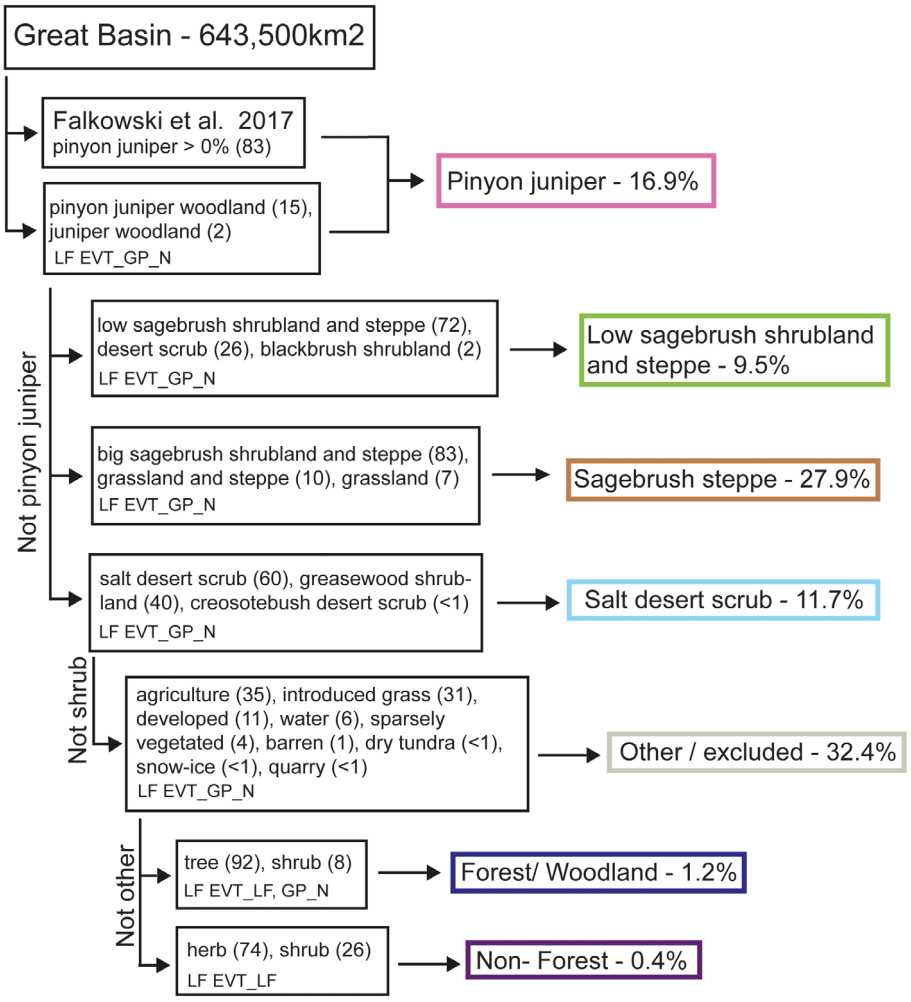

Fig. 1. Schematic of land cover classification. All pinyon-juniper pixels were classified first. The remaining pixels were reclassified based on their LANDFIRE EVT vegetation group (LF EVT_GP_N) classifications. Non-woodland, non-shrubland pixels were classified based on the dominant life form (LF EVT_LF) of that pixel. The vegetation groups within each final classification are listed in order of prevalence within the group, with the percent total in that group in parentheses.

Moisture or Water Index (NDMI; Gao 1996), and the Normalized Burn Ratio (NBR; Key and Benson 2006). This model also included topographic predictors derived from the National Elevation Dataset including elevation, slope, and the sine and cosine of aspect. We then predicted pinyon-juniper canopy cover for 2014 Landsat imagery using the random forest model. We used the resulting estimates of canopy cover to calculate aboveground biomass of pinyon-juniper woodlands that were outside of the extents of the high-resolution maps created by Falkowski et al. (2017*a*). Image preparation and modeling for this stage was performed in Google Earth Engine (Gorelick et al. 2017), a geospatial cloud computing platform.

Any pixel that had >0% pinyon-juniper cover in the Falkowski et al. (2017*a*) product was designated as pinyon-juniper regardless of that LANDFIRE classification in that pixel because of the higher carbon content of trees in comparison with other plant functional types. Pixels that were designated as pinyon-juniper in LANDFIRE EVT but were not designated as pinyon-juniper by

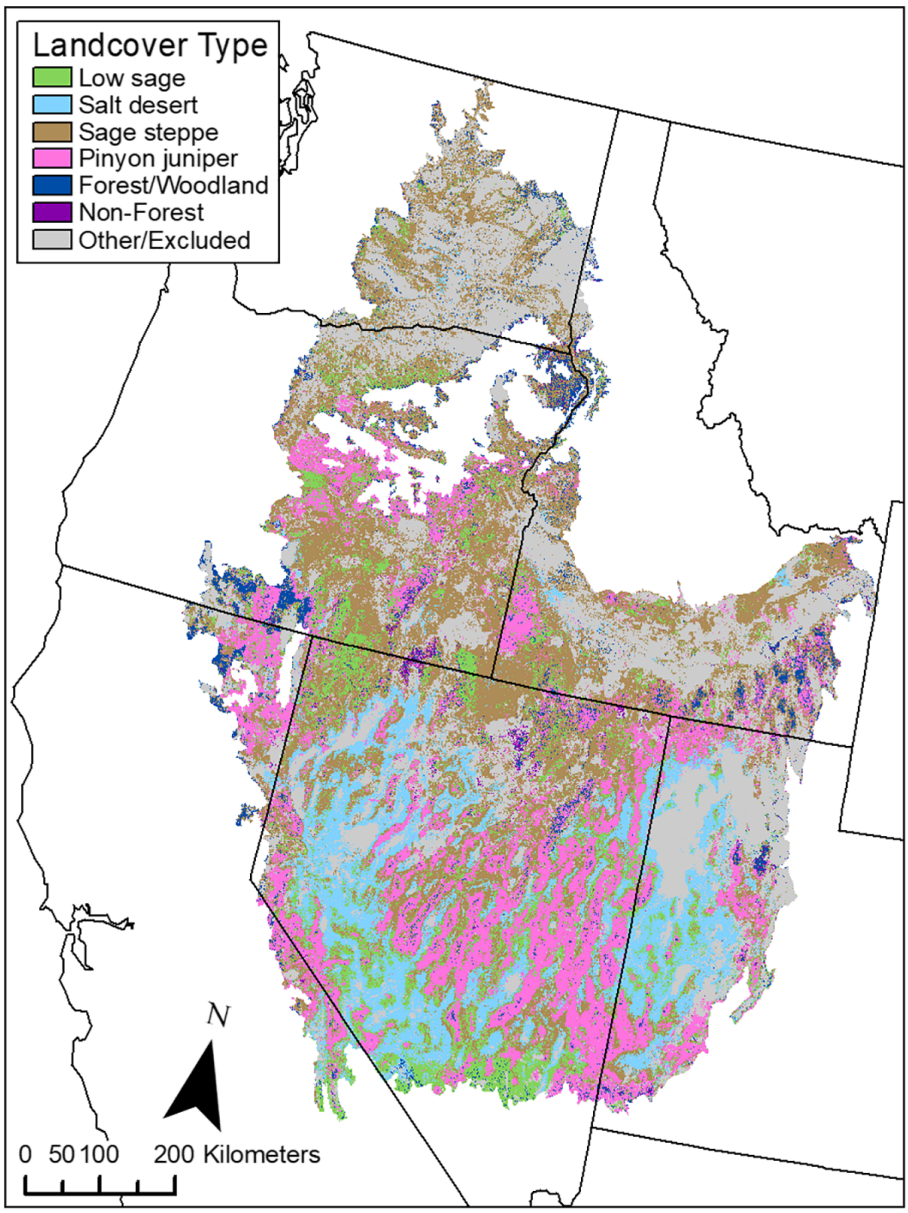

Fig. 2. Land cover classification for the Great Basin based on a combination of woodland cover from Falkowski et al. (2017*a*, *b*) and other land covers from LANDFIRE (Rollins 2009, LANDFIRE 2014).

Falkowski et al. (2017*a* or 2017*b*) were classified as pinyon-juniper with a percent cover estimate of 0.

Carbon estimation for pinyon-juniper

Total aboveground carbon as a function of tree canopy cover was derived using data from 480 (0.10 ha) field plots measured as part of the Sagebrush Steppe Treatment Evaluation Project (SageSTEP; McIver et al. 2014). Components in the estimate of aboveground carbon included tree biomass, tree litter, shrub biomass, standing herbaceous biomass, down woody debris, and shrub/herbaceous litter. Individual tree carbon was estimated based on crown area using allometric equations derived from destructively

harvesting trees from various size classes (see Tausch 2009, Rau et al. 2012 for detailed methods). Individual tree estimates were summed to estimate tree carbon at the plot level.

Tree litter carbon was estimated by placing three 0.25 × 0.25 m sampling frames under six representative trees in each plot. Sampling frames were placed adjacent to the tree stem, halfway between the stem and the canopy edge, and at the canopy edge. All material inside the frame was cut using a handsaw, collected, dried, and weighed. The carbon content of tree litter was estimated by grinding subsamples of the dry litter and analyzing for percentage C via combustion analyzer (Rau et al. 2010, 2012). The total mass of tree litter carbon per plot was estimated by calculating the mass of tree litter carbon per unit area collected and then extrapolating to the total area of litter mat within each plot based on known relationships between tree crown area and litter mat area (Rau et al. 2010, 2012).

Shrub biomass was estimated by measuring the total height, longest crown diameter, and diameter perpendicular to the longest diameter of each shrub intersecting a 2 m wide belt along the 5-, 15-, and 25-m transects, and then applying species-specific allometric equations derived by destructively harvesting shrubs of variable size classes within each species (Reiner et al. 2010). Carbon content of shrubs was estimated by collecting stem, branch, and foliage samples from representative species and obtaining estimates of percentage C by combustion analyzer (Rau et al. 2010, 2012).

Herbaceous biomass, litter biomass, and carbon were estimated in eight total 0.25 × 0.25 m quadrats along two 33-m transects within each plot. Standing herbaceous biomass was clipped at ground level, collected, dried, and weighed, and subsamples were analyzed for percentage C (Rau et al. 2010, 2012). Herbaceous and shrub litter were also collected, dried, and weighed, and subsamples were analyzed for percentage C (Rau et al. 2010, 2012). Down woody debris (DWD) biomass and C were estimated using the planar intercept method on the 5-, 15-, and 25-m transects, where all woody debris >0.635 cm was inventoried where it intersected each transect (Brown 1974); representative DWD subsamples were analyzed for percentage C via combustion analyzer (Rau et al. 2010, 2012).

The sum of aboveground carbon per plot was estimated as the sum of Tree C + Shrub C + Standing Herbaceous C + Down Woody Debris C + Tree, Shrub, and Herbaceous Litter C. The mass of total aboveground carbon per plot was then regressed against tree canopy cover using SAS 9.4 PROC REG (SAS Institute, Cary, North Carolina, USA). The best-fit model (polynomial) was chosen using adjusted R-squared and AIC.

Carbon estimation in three shrubland land cover types

For each of the three shrubland categories, we created a static carbon estimate and applied a stratify & multiply approach to map aboveground carbon (Goetz et al. 2009). These estimates were calculated using data from 455 (0.10 ha) field plots measured as part of the SageSTEP Project (McIver et al. 2014). The vast majority (430) of these plots were categorized as sagebrush steppe (Fig. 1). These plots all contained basin big sagebrush (*Artemisia tridentata*) or Wyoming sagebrush (*Artemisia tridentata* ssp. *wyomingensis*), but also commonly contained a mix of low sagebrush (*Artemisia arbuscula*) and salt desert shrub (*Atriplex* spp.; *Sarcobatus* spp.). In order to quantify unique communities of low sagebrush and salt desert shrub, we measured 25 supplemental plots (10 low sagebrush, 10 greasewood, 5 saltbrush) adjacent to or near the primary SageSTEP plots. All plots were of identical dimensions to the woodland plots described above (30 × 33 m), and all carbon measurements were identical with the exclusion of those associated with trees. The sum of aboveground carbon per plot was estimated as the sum of Shrub C + Standing Herbaceous C + Down Woody Debris C + Shrub and Herbaceous Litter C. For each unique shrub type, the mean aboveground C and standard error were calculated. The mean and standard error were used to create low, medium, and high carbon estimates for each of the three shrubland categories.

Carbon estimates for forest, non-forest, and other

For the other forest/woodland land cover types, we created static estimates using aboveground biomass data from A. T. Hudak et al., *unpublished data*. These data were created using a two-step approach. First, a random forest regression model was created using forest inventory data

and co-located LiDAR measurements to calibrate LiDAR estimates of aboveground biomass. Second, topography (e.g., slope), climate (e.g., mean annual temperature), and Landsat-derived spectral indices (e.g., tasseled cap greenness) were used as training data in a second random forest model to predict the LiDAR-derived aboveground biomass estimates. This model was used to map aboveground biomass in forested land across the Pacific Northwest. Because these data do not cover our entire study area (Appendix S1: Fig. S2), we created 3049 random points in forest land cover within overlapping areas and extracted biomass (Hudak et al., *unpublished data*) and land cover (LANDFIRE.US_140EVT GP_N; Rollins 2009, LANDFIRE 2014). We used these values to calculate the average aboveground biomass associated with each LANDFIRE vegetation classification. Because data from Hudak and colleagues only encompass the northern half of our study region, we standardized these values based on the percent total area of each LANDFIRE vegetation group for the entire study region. These estimates refer to total aboveground biomass, so we divided them by two to convert them to aboveground carbon (biomass is roughly 48–50% carbon). This general conversion is common when converting biomass to carbon (e.g., Saatchi et al. 2011, Kellndorfer et al. 2013). Lastly, pixels that were designated as non-forest or other/excluded were assigned a carbon value of 0.

Comparison to the national biomass and carbon dataset

We compared our results to the National Biomass and Carbon Dataset version 2 (NBCD; Kellndorfer et al. 2013) a national-scale, 30-m regression tree modeled biomass for the United States. The NBCD uses USDA Forest Inventory and Analysis (FIA) data, interferometric synthetic-aperture radar (InSAR) data from the 2000 Shuttle Radar Topography Mission (SRTM), and remote sensing data from Landsat ETM+ to create a regression tree modeled biomass and carbon baseline dataset for the year 2000 (Kellndorfer et al. 2013). This dataset is widely used and was chosen for our comparison in order to assess how well a forest carbon-focused product represented the woodland and shrubland ecosystem characteristic of our dryland study area. We downloaded the tiles that make up the Great Basin region and mosaicked them using the maximum value in places where these tiles may overlap. We randomly selected 5000 points within our study area and extracted our carbon values and the NBCD biomass values, which we divided by two to estimate carbon. We also extracted our classification of land cover for each point. Because both our carbon estimates and the NBCD carbon estimates on pinyon-juniper are continuous values, we created a linear model using just the randomly selected points associated with the pinyon-juniper land cover type (n = 855). For the remaining categories with static carbon estimates, we created boxplots of the NBCD carbon data for each land cover type to compare our estimates.

Results

Land cover classifications in the Great Basin

We classified seven types of land cover in the Great Basin (Fig. 1). Of the land cover categories of interest for carbon accounting, sagebrush steppe was the most extensive, making up roughly 27% of our study area, followed by pinyon-juniper woodland (17%), salt desert shrub (12%), and low sagebrush (10%). The other forest and other non-forest categories made up 1.2% and 0.4%, respectively. Roughly one-third (~32%) of the Great Basin was excluded from carbon accounting because it was classified as agricultural, introduced grass, barren, developed, or water, which should account for very little aboveground carbon (Fig. 2).

Validation of pinyon-juniper percent cover product

Overall, the modeled canopy cover product values ranged from 0% to 92% cover (mean = 15.3%). Of the pixels classified as pinyon-juniper, about 44% had less than 10% canopy cover, and about 79% had less than 25% canopy cover. The 265 SageSTEP control plots encompass a large range of cover from 0% to 75.7% (mean $\pm$ SE = 14.9 $\pm$ 1.1) and are distributed across the study region (Appendix S1: Fig. S1). Based on the linear regression comparison to the 30-m tree cover estimates derived from Falkowski et al. (2017*a*), modeled pinyon-juniper cover from aerial photographs shows a

reasonably strong correlation with field-based measurements (R^2 = 0.62; Fig. 3).

There were 23 data points with a pinyon-juniper cover discrepancy of greater than 20%. SageSTEP field estimates were higher in 17 of these plots (SageSTEP mean ± SE = 54.9 ± 2.4; Canopy cover model mean ± SE = 22.7 ± 1.2), suggesting that the mapped data may have a tendency to underestimate total pinyon-juniper in areas of high cover (Appendix S1: Fig. S3). Visual inspection of the 17 underestimated SageSTEP plots in conjunction with the original 1-m resolution data and NAIP imagery also suggests that some tree canopies were omitted in the modeled canopy estimates (Appendix S1: Fig. S4). The SageSTEP plots that recorded less than 2% cover difference tended to be in areas of relatively low pinyon-juniper cover (n = 139, mean ± SE = 3.54 ± 0.74), suggesting that our cover estimates are most accurate in areas of low cover.

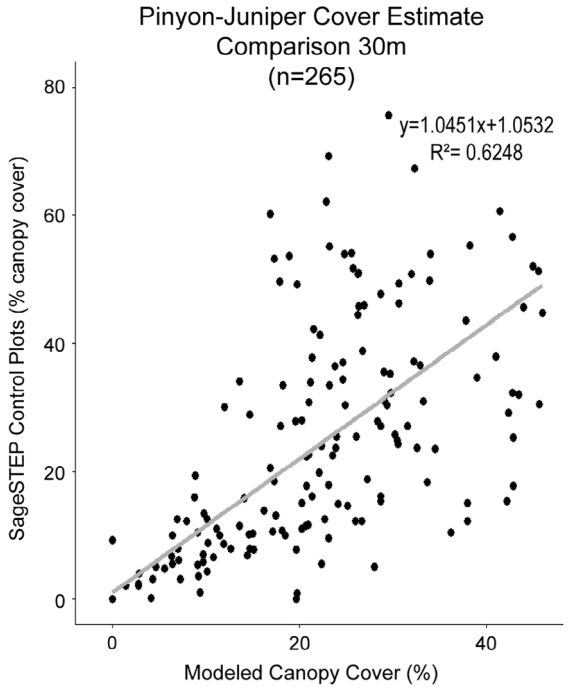

Fig. 3. Modeled pinyon-juniper canopy cover showed a strong, positive relationship (R^2 = 0.62) with SageSTEP field measurements of pinyon-juniper percent cover. Canopy cover estimates were aggregated to a 30 m pixel size, which corresponds to the SageSTEP plot size.

Carbon estimates for land cover classes

Based on the SageSTEP field measurements of canopy cover and aboveground biomass C, we developed a cover-based equation of total aboveground carbon for pixels designated as pinyon-juniper. The equation has high explanatory power and shows a strong positive relationship between percent canopy cover and total aboveground carbon (n = 1148, r^2 = 0.94, P < 0.001; Fig. 4). Although the equation has a polynomial form, the linear coefficient determines the bulk of the relationship. The non-zero intercept value of 3153 kg/ha represents carbon associated with shrubs and herbaceous biomass growing within woodland communities where pinyon-juniper canopy cover is very low or absent.

Mean estimates of total aboveground carbon for the three shrubland categories ranged from 3056 kg/ha in salt desert shrub to 3778 kg/ha in low sagebrush, with estimates much more robust in the well-sampled sagebrush steppe. Estimated value for total aboveground carbon for the other forest was 27,511 kg/ha based on aboveground biomass data from Hudak et al. (*unpublished data*; Table 1). The other non-forest category was assigned a value of 0 kg/ha.

Total Great Basin carbon estimates

Based on our models, we estimated that there was a total of 295.4 Tg of aboveground carbon in the Great Basin circa 2014 when using mean carbon estimates for the three shrubland categories (Table 2, Fig. 5). While the pinyon-juniper land

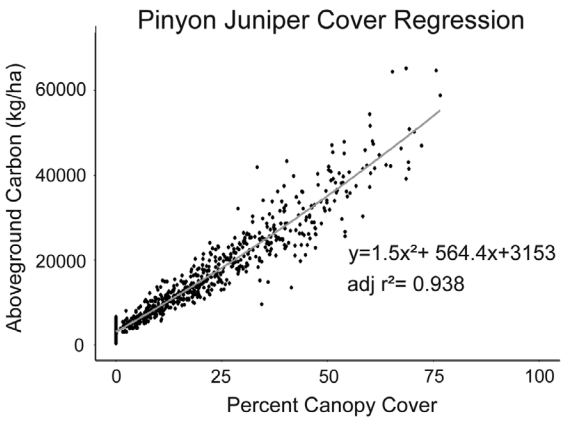

Fig. 4. Total aboveground carbon in pinyon-juniper is strongly related to canopy cover.

Table 1. Carbon per pixel calculated for each land cover type.

Land cover type	Total kg carbon/ha
Pinyon-juniper	$1.5x^2 + 564.4x + 3153$
Forest	27,511
Sagebrush steppe	3067 (3011–3122)
Low sagebrush	3778 (2778–4789)
Salt desert shrub	3056 (2500–3622)
Non-forest	0
Excluded	0

Notes: The three shrubland categories (low sagebrush, salt desert, and sagebrush steppe) have a mean carbon estimate followed by a low and high estimate based on the standard error. Pinyon-juniper is calculated as a function of canopy cover per pixel (x).

cover type comprises only 16.9% of the Great Basin by total area, it accounted for 43.7% of the total aboveground carbon (Table 2). When the three shrubland categories were combined, they account for roughly half of the total land area (49.1%) and contribute 34.3% of the total aboveground carbon estimated for the study area.

Comparison to the national biomass and carbon dataset

The relationship between our estimates of carbon in pinyon-juniper land cover vs. the NBCD data was significant, but weak ($R^2 = 0.14$, $n = 855$; Fig. 6). While carbon was positively correlated between our estimates and the NBCD (Pearson's $r = 0.38$, $n = 855$, $P < 0.001$), the NBCD estimated zero carbon in 20% of the pixels containing pinyon-juniper woodland. For the land cover classes that had fixed, rather than continuous, carbon estimates, our carbon estimate was higher in all cases with the exception of the non-forest and other classifications which we had assigned a zero value (Fig. 7). Total carbon in the Great Basin based on NBCD estimates is 161 Tg, which accounts for only 54.5% of the total carbon in our modeled estimates.

Table 2. Total area and teragrams (Tg) of carbon by land cover type using mean estimates for the shrubland categories.

Land cover type	Total area (%)	Total carbon (Tg)
Pinyon-Juniper	16.9	129.1
Forest	1.2	65.0
Sagebrush steppe	27.9	55.0
Low sagebrush	9.5	23.2
Salt desert shrub	11.7	23.1
Non-forest	0.4	0
Excluded	32.4	0
Total	100	295.4

Discussion

Carbon accounting is increasingly important as we aim to combat climate change by reducing deforestation and degradation of terrestrial ecosystems. To date, aboveground carbon models have largely neglected semi-arid regions and those that have estimated carbon have focused on plot-level studies or subsets of ecoregions. Our analysis provides a first comprehensive estimate of aboveground carbon in the Great Basin, a spatially extensive semi-arid region of the western United States. Our results suggest that Great Basin woodland and shrubland ecosystems contain nearly twice the aboveground carbon estimated by the National Biomass and Carbon Dataset. Given that semi-arid ecosystems account for 45% of non-frozen terrestrial lands globally and are at risk for severe degradation from disturbance and exotic species invasion, this analysis underscores the need to better understand carbon storage in these ubiquitous landscapes. Here, we examine factors that may impact our carbon estimates in each land cover type and compare our estimates with previous work in similar regions.

Land cover classifications in the Great Basin

The Great Basin was designated into seven distinct land cover classifications, and these general classifications were based on dominant plant functional groups and their potential contributions to aboveground carbon. In the Great Basin, the most widespread of the shrub-steppe communities is the basin big sagebrush steppe, and we originally hypothesized that these communities would have higher productivity and carbon storage than the other shrub types. Our results indicate that although highly variable and dependent on local conditions, the salt desert shrub and low sagebrush types can produce similar carbon storage estimates when compared to sagebrush steppe. To better characterize the variance in shrubland carbon estimates, additional research may be needed to relate shrub canopy

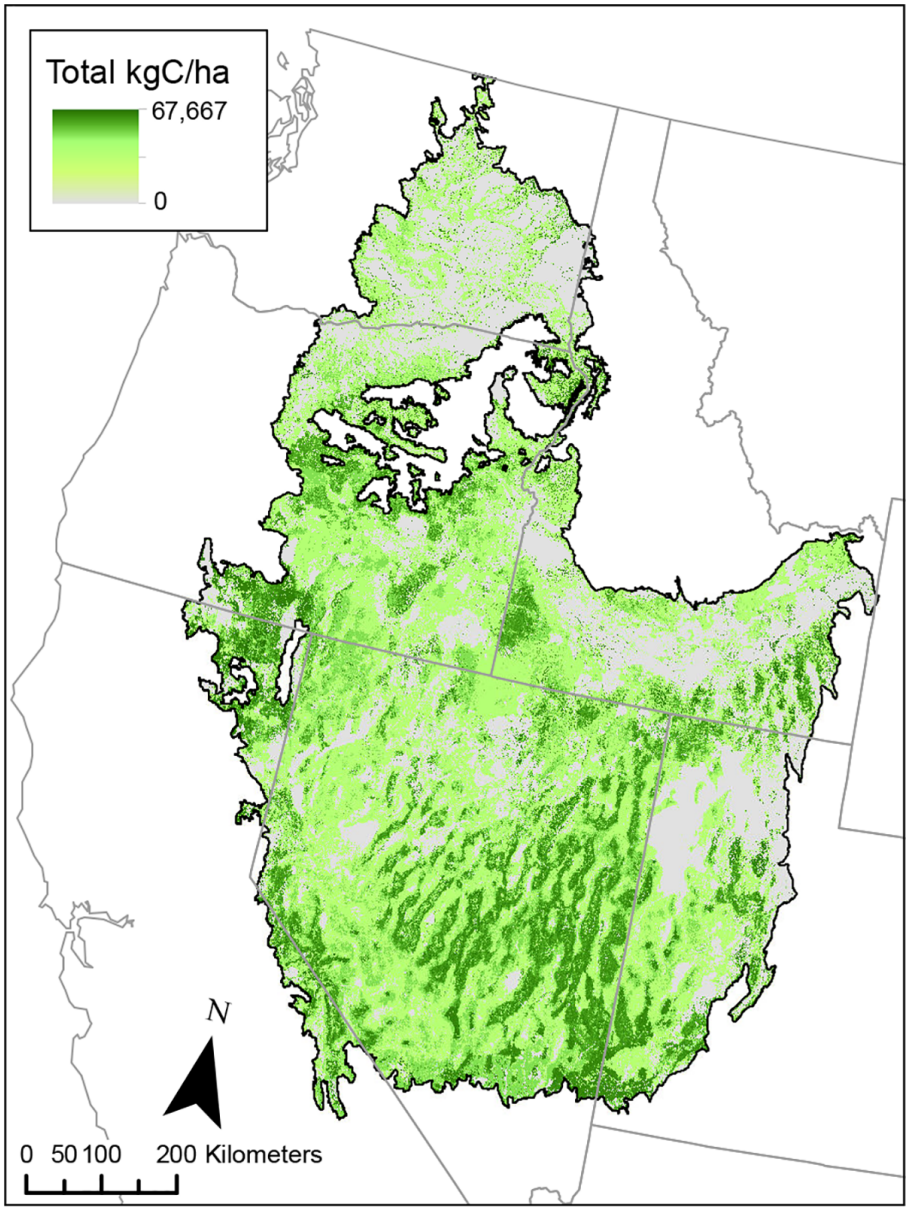

Fig. 5. Estimated aboveground biomass carbon storage in the Great Basin (kg/ha) using mean estimates for the three shrubland categories.

cover and height to biomass and carbon estimates (e.g., Anderson et al. 2018).

Pinyon-juniper carbon

Our results comparing the remotely sensed pinyon-juniper percent cover product (Falkowski et al. 2017*a*) with canopy cover estimates from SageSTEP plots (McIver et al. 2014) are consistent with previous validation work that suggests a tendency of underestimation in high cover areas (Poznanovic et al. 2014, Falkowski et al. 2017*a*). This was particularly pronounced in areas where SageSTEP plots measured >50% cover (Appendix S1: Fig. S2). Our estimates of pinyon-juniper canopy cover (mean ± SE = 15.1 ± 0.4, range = 0–65.8%, n = 855) are similar

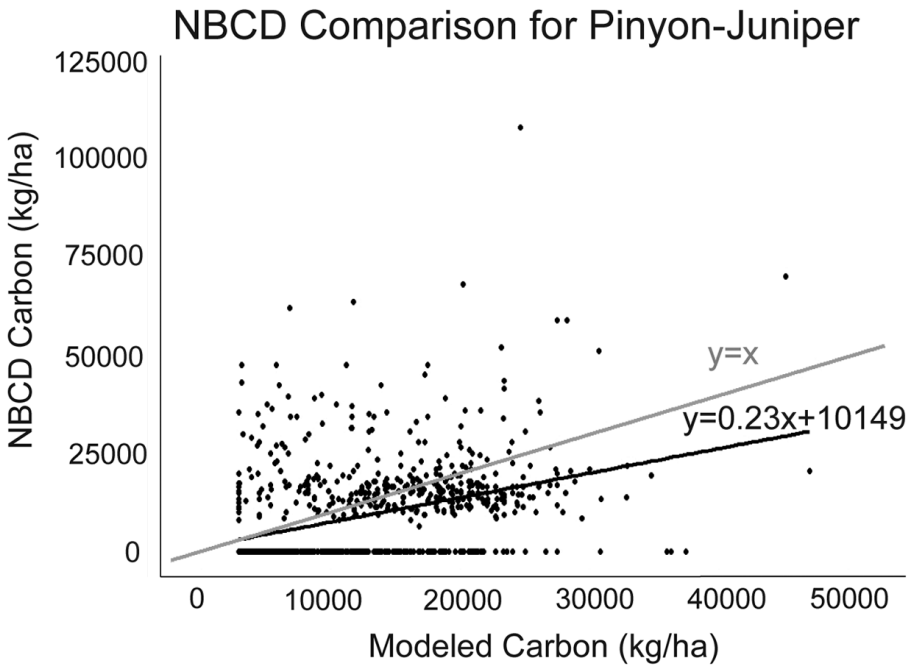

Fig. 6. Regression of pinyon-juniper carbon estimates from our map compared to the National Biomass and Carbon Dataset for a random sample (n = 855). There was a weak but significant positive relationship (R^2 = 0.147, P < 0.01).

to remotely sensed estimates of pinyon-juniper systems in the Colorado Plateau (mean = 22%, range = 0–58.9%; Huang et al. 2009) which used a multiscale approach including field measurements, airborne imaging, and Landsat satellite data, suggesting that our estimates are a reasonable representation of canopy cover at regional scales.

Our estimate of total carbon in Great Basin pinyon-juniper systems (~11,883 ± 7238 kgC/ha; mean ± SD of all pixels designated as pinyon-juniper) is also within the range of Huang et al. (2009) who estimated a total of 19,240 ± 7400 kgC/ha (mean ± SD) in pinyon-juniper systems in the Colorado Plateau, and this variation could reflect actual differences in the pinyon-juniper carbon contributions in these different locations. Finally, our estimate of total pinyon-juniper carbon in the Great Basin may also be conservative given the tendency of the canopy cover map to underestimate the high cover field measurements obtained from the SageSTEP project.

Although our canopy cover model may underestimate aboveground carbon, our land cover map might overestimate the extents of woodland ecosystems. This is because much of our pinyon-juniper classification was based on data from Falkowski et al. (2017*a*, *b*) where any pixel with >0% pinyon-juniper cover was designated as pinyon-juniper. These designations superseded cover classifications from LANDFIRE in order to better capture the higher carbon content of trees, and therefore, our maps likely represent the maximum land area of pinyon-juniper ecosystems present in the Great Basin. This is illustrated in the high amount of pinyon-juniper area in our land cover map (16.9%) compared to the LANDFIRE map alone (8.2%). In addition, our land cover map estimates 19.7% pinyon-juniper cover compared to 14.6% in the same geographic area in previous work (Bradley and Mustard 2008). This overestimation, however, should have little impact on the overall carbon estimate in the Great Basin because areas of <5% pinyon-juniper cover have carbon estimates similar to those in shrubland ecosystems. While classifying all pixels with any pinyon-juniper vegetation as pinyon-juniper is useful for carbon estimates

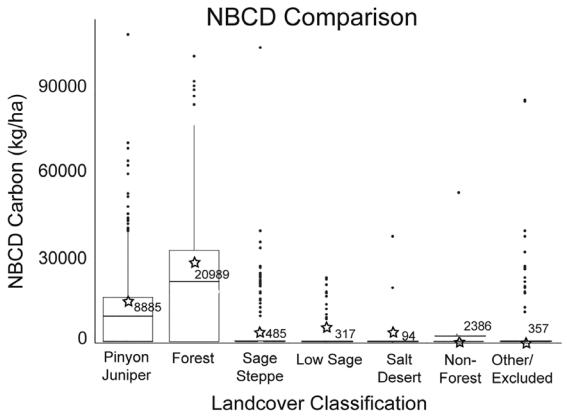

Fig. 7. For six land cover classes, we provided static carbon estimates (stars; values in Table 1). The boxplots show mean estimates of carbon from a random sample of the NBCD (n = 4145). Most of the pixels in the associated NBCD for these land cover types had values of 0, with means ranging from 94 to 20,989 kg/ha. All means (denoted by a line in each boxplot) in the NBCD were lower than the static estimates with the exception of the other/excluded and non-forest classifications. The stars represent the modeled mean for each land cover type. The modeled mean for pinyon-juniper is 12,222 ± 7408 kgC/ha (mean ± SD) and refers to the mean of the 855 pinyon-juniper designated points included in the comparison analysis.

because they are the most significant contributor to carbon on this landscape, this approach could be problematic if used for mapping habitat for pinyon-juniper specialist species.

Carbon in other land covers

Each of the remaining six land cover classes in the Great Basin was given a static carbon estimate based on field sampling (shrubland) or remotely sensed products (forest). Estimates of aboveground carbon for the low sagebrush and sagebrush steppe shrubland categories are similar to estimates of aboveground biomass for these shrubland ecosystems in previous work (Rickard 1985, Bradley et al. 2006), and salt desert is slightly higher (Driese and Reiners 1997, Bradley et al. 2006). Because of the high variability in the low sagebrush and salt desert shrub ecosystems partially due to low sample size, we also calculated aboveground carbon estimates using a range of shrubland carbon values. Overall aboveground carbon estimates ranged from 284.0 Tg to 306.9 Tg when calculating totals based on low and high shrubland carbon estimates, suggesting that errors in the shrub estimates have minimal effect on the estimate of overall carbon in the Great Basin.

The forest land classification was assigned carbon values using remotely sensed aboveground biomass data (Hudak et al., *unpublished data*), and our estimate for forest aboveground carbon is similar to previous estimates of forest carbon (Kellndorfer et al. 2013; Fig. 7). While the non-forest land cover category likely has more carbon than the assigned 0 value, it is defined largely by grassland and only accounts for 0.4% of the total study area, suggesting that this land cover category does not have a big impact on the overall carbon storage within the Great Basin region.

While the excluded land cover category made up roughly one-third of the Great Basin, we do not expect that this will significantly impact the overall aboveground carbon storage estimates. Our excluded category included primarily agriculture, introduced grass, development, and water. These vegetation types typically store small amounts of aboveground carbon. For example, in the Great Basin, introduced grassland is primarily cheatgrass which has aboveground carbon typically below 1000 kgC/ha (Bradley et al. 2006, Diamond et al. 2012, Kessler et al. 2015). While on average, agriculture systems in the United States store some carbon, it is typically harvested, resulting in little long-term aboveground carbon storage.

Total Great Basin carbon estimates

Previous work by Kellndorfer et al. (2013) estimated aboveground carbon storage in the Great Basin at 161 Tg, but our regional estimate of carbon is nearly double this amount (295.4 Tg). While the NBCD provides a baseline estimate for carbon in the year 2000, and our data reflect carbon storage during roughly 2011–2014, the differences in these carbon maps are not likely due to actual changes in carbon storage alone. Instead, our estimates are likely higher because they focus on shrubland and woodland aboveground carbon, which collectively make up 66% of the land area (230.4 Tg C) in the Great Basin, while Kellndorfer and colleagues only account for carbon in forest designated pixels of the same

region. In addition, Kellndorfer and colleagues reported a strong correlation between modeled carbon and carbon measured in forested FIA plots in the areas included in our Great Basin study map (r = 0.44–0.86). However, the correlation with our modeled pinyon-juniper data (Pearson's $r = 0.38$, $n = 855$, $P < 0.001$) was weaker. These discrepancies are not surprising, because most land within the Great Basin is not considered forest (at least 10% tree cover), and Kellndorfer et al. (2013) only mapped 1–65% of their subregions within our study area. Plots typically must have at least 10% forest cover for a forest designation in the FIA dataset, which was used to train the NBCD (Kellndorfer et al. 2013). Since nearly half (44%) of our pinyon-juniper pixels were estimated to have less than 10% cover, their exclusion may be a major reason for the differences in carbon accounting between the two products. In fact, 20% of our randomly selected pinyon-juniper pixels were identified as containing 0 kg C by Kellndorfer et al. (2013), likely because they were not considered forest and were not mapped. This suggests that national- and global-scale carbon accounting products focused on forest carbon are poorly suited for estimating carbon in semi-arid ecosystems where woodland and shrubland carbon storage may be substantial. We recommend that researchers and managers working on carbon storage in dryland regions globally exercise caution when using forest-focused carbon maps.

Product applications and management implications

The Great Basin is a region undergoing rapid and extensive land cover change. In some areas, expansion of woody vegetation, including pinyon-juniper woodland, is common (Miller et al. 2008, Wang et al. 2018). However, aboveground carbon storage in ecosystems is increasingly threatened by fire and conversion to non-native annual grasslands (Bradley et al. 2006, Balch et al. 2013) and has a history of large-scale alteration of ecosystems due to livestock grazing (Branson 1953, Hickey 1961, Mack and Thompson 1982, Young et al. 1987). By creating a robust, spatially explicit estimate of aboveground carbon storage in Great Basin ecosystems, this analysis provides an important first step toward measuring and accounting for carbon changes through degradation of this extensive semi-arid region.

Acknowledgments

This is Contribution Number 131 of the Sagebrush Steppe Treatment Evaluation Project (SageSTEP), funded by the US Joint Fire Science Program, the Bureau of Land Management, the National Interagency Fire Center, and the Great Northern Landscape Conservation Cooperative. Funding was also provided by NASA award number NNH15AZ06I and Joint Venture Agreement 16-JV-11221633-061. We thank Patrick Fekety and Andrew Hudak for providing maps of forest carbon. We thank Gabriella Saloio for her contributions to initial data processing. We also thank two anonymous reviewers for their comments.

Literature Cited

Ahlström, A., et al. 2015. The dominant role of semi-arid ecosystems in the trend and variability of the land CO_2 sink. Science 348:895–899.

Anderson, K. E., N. F. Glenn, L. P. Spaete, D. J. Shinneman, D. S. Pilliod, R. S. Arkle, S. K. McIlroy, and D. R. Derryberry. 2018. Estimating vegetation biomass and cover across large plots in shrub and grass dominated drylands using terrestrial lidar and machine learning. Ecological Indicators 84:793–802.

Baccini, A., N. Laporte, S. J. Goetz, M. Sun, and H. Dong. 2008. A first map of tropical Africa's aboveground biomass derived from satellite imagery. Environmental Research Letters 3:1–9.

Balch, J. K., B. A. Bradley, C. M. D'Antonio, and J. Gómez-Dans. 2013. Introduced annual grass increases regional fire activity across the arid western USA (1980–2009). Global Change Biology 19:173–183.

Blaisdell, J. P., and R. C. Holmgren. 1984. Managing intermountain rangelands- salt-desert shrub ranges. General Technical Report INT-163. USDA Forest Service Intermountain Forest and Range Experiment Station, Ogden, Utah, USA.

Bradley, B. A. 2010. Assessing ecosystem threats from global and regional change: hierarchical modeling of risk to sagebrush ecosystems from climate change, land use, and invasive species in Nevada, USA. Ecography 33:198–208.

Bradley, B. A., R. A. Houghton, J. F. Mustard, and S. P. Hamburg. 2006. Invasive grass reduces aboveground carbon stocks in shrublands of the Western US. Global Change Biology 12:1815–1822.

Bradley, B. A., and J. F. Mustard. 2008. Comparison of phenology trends by land cover class: a case study

in the Great Basin, USA. Global Change Biology 14:334–346.

Branson, F. A. 1953. Two new factors affecting resistance of grasses to grazing. Journal of Range Management 6:165–171.

Brooks, M. L., and J. C. Chambers. 2011. Resilience to fire in desert shrublands of North America. Rangeland Ecology & Management 64:431–438.

Brown, J. K. 1974. Handbook for inventorying downed woody material. General Technical Report INT-16. USDA Forest Service Intermountain Forest & Range Experiment Station, Ogden, Utah, USA.

Campbell, J. L., R. E. Kennedy, W. B. Cohen, and R. F. Miller. 2012. Assessing the carbon consequences of western juniper (*Juniperus occidentalis*). Rangeland Ecology & Management 65:223–231.

Cartus, O., J. Kellndorfer, W. Walker, C. Franco, J. Bishop, L. Santos, and J. M. M. Fuentes. 2014. A national, detailed map of forest aboveground carbon stocks in Mexico. Remote Sensing 6:5559–5588.

Chambers, J. C., B. A. Bradley, C. S. Brown, C. D'Antonio, M. J. Germino, J. B. Grace, S. P. Hardegree, R. F. Miller, and D. A. Pyke. 2014. Resilience to stress and disturbance, and resistance to *Bromus tectorum* L. invasion in cold desert shrublands of western North America. Ecosystems 17:360–375.

Chojnacky, D. C., S. P. Prisley, and S. R. Miller. 2012. Linking forest inventory and analysis ground data to maps: an example for Nevada pinyon-juniper forests. Western Journal of Applied Forestry 27:118–127.

Diamond, J. M., C. A. Call, and N. Devoe. 2012. Effects of targeted grazing and prescribed burning on community and seed dynamics of a downy brome (*Bromus tectorum*)–dominated landscape. Invasive Plant Science and Management 5:259–269.

Driese, K. L., and W. A. Reiners. 1997. Aerodynamic roughness parameters for semi-arid natural shrub communities of Wyoming, USA. Agricultural and Forest Meteorology 88:1–14.

Falkowski, M. J., J. S. Evans, D. E. Naugle, C. A. Hagen, S. A. Carleton, J. D. Maestas, A. H. Khalyani, A. J. Poznanovic, and A. J. Lawrence. 2017*a*. Mapping tree canopy cover in support of proactive prairie grouse conservation in western North America. Rangeland Ecology & Management 70:15–24.

Falkowski, M. J., A. T. Hudak, S. K. Filippelli, and P. A. Fekety. 2017*b*. Developing a carbon monitoring system for pinyon-juniper forests and woodlands. Presented at the American Geophysical Union, Fall Meeting, New Orleans, Louisiana, USA. Retrieved from https://agu.confex.com/agu/fm17/meetingapp.cgi/Paper/295240

Federal Geographic Data Committee. 2008. The National Vegetation Classification Standard, Version 2. FGDC Vegetation Subcommittee. FGDC-STD-005-2008 (Version 2).

Gao, B. 1996. NDWI a normalized difference water index for remote sensing of vegetation liquid water from space. Remote Sensing of Environment 58:257–266.

GAP/USGS. 2016. LANDFIRE/GAP Land Cover Map Unit Descriptions: 1–1377.

Goetz, S. J., A. Baccini, N. T. Laporte, T. Johns, W. Walker, J. Kellndorfer, R. A. Houghton, and M. Sun. 2009. Mapping and monitoring carbon stocks with satellite observations: a comparison of methods. Carbon Balance and Management 4:1–7.

Gorelick, N., M. Hancher, M. Dixon, S. Ilyushchenko, D. Thau, and R. Moore. 2017. Google earth engine: planetary-scale geospatial analysis for everyone. Remote Sensing of Environment 202:18–27.

Gray, J. T. 1982. Community structure and productivity in ceanothus chaparral and coastal sage scrub of southern California. Ecological Monographs 52:415–435.

Haverd, V., A. Ahlström, B. Smith, and J. G. Canadell. 2017. Carbon cycle responses of semi-arid ecosystems to positive asymmetry in rainfall. Global Change Biology 23:793–800.

Hengeveld, G. M., K. Gunia, M. Didion, S. Zudin, A. P. P. M. Clerkx, and M. J. Schelhaas. 2015. Global 1- degree maps of forest area, carbon stocks, and biomass, 1950–2010. ORNL DAAC, Oak Ridge, Tennessee, USA.

Hickey, W. C. 1961. Growth form of crested wheatgrass as affected by site and grazing. Ecology 42:173–176.

Houghton, R. A. 2007. Balancing the global carbon budget. Annual Review of Earth and Planetary Sciences 35:313–347.

Huang, A. C., G. P. Asner, R. E. Martin, N. N. Barger, and J. C. Neff. 2009. Analysis of tree cover and aboveground carbon stocks in pinyon-juniper woodlands. Ecological Applications 19:668–681.

Kellndorfer, J., W. Walker, K. Kirsch, G. Fiske, J. Bishop, L. Lapoint, M. Hoppus, and J. Westfall. 2013. NACP aboveground biomass and carbon baseline data, V.2 (NBCD 2000), U.S.A., 2000. ORNL DAAC, Oak Ridge, Tennessee, USA.

Kessler, K. C., S. J. Nissen, P. J. Meiman, and K. G. Beck. 2015. Litter reduction by prescribed burning can extend downy brome control. Rangeland Ecology & Management 68:367–374.

Key, C. H., and N. C. Benson. 2006. Landscape assessment. *In* D. C. Lutes, R. E. Keane, J. F. Caratti, C. H. Key, N. C. Benson, S. Sutherland, and L. J. Gangi, editors. FIREMON: fire effects monitoring

and inventory system. General Technical Report. 164-CD:LA1–LA51. USDA Forest Service Rocky Mountain Research Station, Fort Collins, Colorado, USA.

Lal, R. 2004. Carbon sequestration in dryland ecosystems. Environmental Management 33:528–544.

LANDFIRE. 2014. Existing Vegetation Type Layer, LANDFIRE 1.4.0, U.S. Department of the Interior, Geological Survey. https://www.landfire.gov/version_comparison.php?mosaic=Y

Mack, R. N., and J. N. Thompson. 1982. Evolution in Steppe with few large, hooved mammals. American Naturalist 119:757–773.

McArthur, E. D., and J. R. Taylor. 2004. *Artemisia arbuscula* Nutt. low sagebrush. *In* Wildland shrubs of the United States and its territories: thamnic descriptions: volume 1. General Technical Report IITF-GTR26:1–844. USDA Forest Service, International Institute of Tropical Forestry, San Juan, Puerto Rico, USA; Rocky Mountain Research Station, Fort Collins, Colorado, USA.

McIver, J., et al. 2014. A synopsis of short-term response to alternative restoration treatments in sagebrush-steppe: the SageSTEP project. Rangeland Ecology and Management 67:584–598.

Miller, R. F., R. J. Tausch, E. D. McArthur, D. D. Johnson, and S. C. Sanderson. 2008. Age structure and expansion of pinyon-juniper woodlands: a regional perspective in the intermountain west. Research Paper Report RMRS-RP-69:1–15. USDA Forest Service Rocky Mountain Research Station, Fort Collins, Colorado, USA.

Poulter, B., et al. 2014. Contribution of semi-arid ecosystems to interannual variability of the global carbon cycle. Nature 509:600–604.

Poznanovic, A. J., M. J. Falkowski, A. L. Maclean, A. M. S. Smith, and J. S. Evans. 2014. An accuracy assessment of tree detection algorithms in juniper woodlands. Photogrammetric Engineering & Remote Sensing 80:627–637.

Rau, B. M., R. Tausch, A. Reiner, D. W. Johnson, J. C. Chambers, and R. R. Blank. 2012. Developing a model framework for predicting effects of woody expansion and fire on ecosystem carbon and nitrogen in a pinyon-juniper woodland. Journal of Arid Environments 76:97–104.

Rau, B. M., R. Tausch, A. Reiner, D. W. Johnson, J. C. Chambers, R. R. Blank, and A. Lucchesi. 2010. Influence of prescribed fire on ecosystem biomass, carbon, and nitrogen in a pinyon juniper woodland. Rangeland Ecology & Management 63:197–202.

Reiner, A. L., R. J. Tausch, and R. F. Walker. 2010. Estimation procedures for understory biomass and fuel loads in sagebrush steppe invaded by woodlands. Western North American Naturalist 70:312–322.

Rickard, W. H. 1985. Biomass and shoot production in an undisturbed sagebrush-bunchgrass community. Northwest Science 59:126–133.

Rollins, M. G. 2009. LANDFIRE: a nationally consistent vegetation, wildland fire, and fuel assessment. International Journal of Wildland Fire 18: 235–249.

Rouse, J. W., R. H. Haas, J. A. Schell, and D. W. Deering. 1974. Monitoring Vegetation Systems in the Great Plains with ERTS, Paper A20. Proceedings of the Third ERTS Symposium: 309–317.

Saatchi, S. S., et al. 2011. Benchmark map of forest carbon stocks in tropical regions across three continents. Proceedings of the National Academy of Sciences 108:9899–9904.

Sankey, T. T., and M. J. Germino. 2008. Assessment of juniper encroachment with the use of satellite imagery and geospatial data. Rangeland Ecology & Management 61:412–418.

Strand, E. K., L. A. Vierling, A. M. S. Smith, and S. C. Bunting. 2008. Net changes in aboveground woody carbon stock in western juniper woodlands, 1946–1998. Journal of Geophysical Research 113: 1–13.

Tausch, R. J. 2009. A structurally based analytic model for estimation of biomass and fuel loads of woodland trees. Natural Resource Modeling 22:463–488.

Tueller, P. T. 1989. Vegetation and land use in Nevada. Rangelands 11:204–210.

U.S. Environmental Protection Agency. 2013. Level III ecoregions of the conterminous United States. U.S. EPA Office of Research & Development (ORD) – National Health and Environmental Effects Research Laboratory (NHEERL). ftp://ftp.epa.gov/wed/ecoregions/us/us_eco_l4.zip, http://edg.epa.gov

U.S. Geological Survey. 2019*a*. Landsat 4-7 Surface Reflectance (Ledaps) Product Guide. (No. LSDS-1370 Version 2.0). Retrieved from https://www.usgs.gov/media/files/landsat-4-7-surface-reflectance-code-ledaps-product-guide

U.S. Geological Survey. 2019*b*. Landsat 8 Surface Reflectance Code (LASRC) Product Guide. (No. LSDS-1368 Version 2.0). Retrieved from https://www.usgs.gov/media/files/landsat-8-surface-reflectance-code-lasrc-product-guide:40

Wang, J., X. Xiao, Y. Qin, R. B. Doughty, J. Dong, and Z. Zou. 2018. Characterizing the encroachment of juniper forests into sub-humid and semi-arid prairies from 1984 to 2010 using PALSAR and Landsat data. Remote Sensing of Environment 205: 166–179.

Young, J. A., R. A. Evans, R. E. Eckert, and B. L. Kay. 1987. Cheatgrass. Rangelands 9:266–270.

Zald, H. S. J., J. L. Ohmann, H. M. Roberts, M. J. Gregory, E. B. Henderson, R. J. McGaughey, and J. Braaten. 2014. Influence of lidar, Landsat imagery, disturbance history, plot location accuracy, and plot size on accuracy of imputation maps of forest composition and structure. Remote Sensing of Environment 143:26–38.

Data Availability

Carbon data generated for this manuscript are available at http://scholarworks.umass.edu/data/101.

Supporting Information

Additional Supporting Information may be found online at: http://onlinelibrary.wiley.com/doi/10.1002/ecs2.2821/full